Cancer Nanotechnology

RESEARCH Open Access

Ultrasmall Fe_3O_4 and Gd_2O_3 hybrid nanoparticles for T_1-weighted MR imaging of cancer

Abolfazl Sarikhani[1,2], Zahra Alamzadeh[1], Jaber Beik[1], Rasoul Irajirad[1], Mehri Mirrahimi[1], Vahid Pirhajati Mahabadi[3], S. Kamran Kamrava[4], Habib Ghaznavi[5*] and Samideh Khoei[1,2*]

*Correspondence: dr.ghaznavi@zaums.ac.ir; khoei.s@iums.ac.ir

[1] Finetech in Medicine Research Center, Iran University of Medical Sciences, Tehran, Iran
[2] Medical Physics Department, Iran University of Medical Sciences, Tehran, Iran
[3] Neuroscience Research Center, Iran University of Medical Sciences, Tehran, Iran
[4] ENT and Head & Neck Research Center and Department, The Five Senses Health Institute, Hazrat Rasoul Akram Hospital, Iran University of Medical Sciences, Tehran, Iran
[5] Pharmacology Research Center, Zahedan University of Medical Sciences, Zahedan, Iran

Abstract

Gadolinium-based contrast agents (GdCAs) have been the most frequently used T_1-weighted magnetic resonance imaging (MRI) contrast agents for decades. However, they have serious disadvantages such as low longitudinal relaxivity value (r_1) and high dose associated-nephrotoxicity that restrict their wide applications. These emphasize the need for an ideal stable and biocompatible T_1-weighted CA with high contrast enhancement performance. Here, we propose a wet-chemical synthesis technique to form a nanocomposite consisting of ultrasmall iron oxide nanoparticles (US-IO) and Gd_2O_3 hybrid nanoparticles stabilized with dextran (FG-HNPs) for T_1-weighted MR imaging. Relaxometry study showed that FG-HNPs have a high r_1 value (42.28 $mM^{-1}S^{-1}$) and low relaxivity ratio (r_2/r_1: 1.416) at 3.0T. In vivo MRI contrast enhancement factor (ΔSNR) for FG-HNPs (257.025 ± 17.4%) was found to be 1.99-fold higher than US-IO (129.102 ± 15%) and 3.35-fold higher than Dotarem (76.71 ± 14.2%) as routinely used T_1-weighted CA. The cytotoxicity assay and histological examination confirmed the biocompatibility of FG-HNPs. The biodistribution study, transmission electron microscopy (TEM) and Prussian blue (PB) staining of tumor tissue proved the effective tumor localization of FG-HNPs. Therefore, FG-HNPs can be suggested as a promising CA for T_1-weighted MRI of tumors by virtue of their remarkable relaxivities and high biocompatibility.

Keywords: T_1-weighted MR imaging, Tumor diagnosis, Hybrid nanoparticles, Contrast agents, Ultrasmall iron oxide nanoparticles

Introduction

Magnetic resonance imaging (MRI) is one of the most powerful non-invasive diagnostic modalities in medical imaging and biomedical research that applies non-ionizing safe radiation, offering deep tissue penetration, high spatial resolution (~ 1 mm) and superior soft-tissue contrast (Ananta et al. 2010; Shen et al. 2018). MRI is used in a wide variety of applications including Alzheimer's disease (Struyfs et al. 2020), angiography (Liu et al. 2018), pH monitoring (Ni et al. 2016), liver diseases (Huang et al. 2014), cell-based therapy (Fink et al. 2018), tumor diagnosis (Han et al. 2017; Zhou

et al. 2021; Mi et al. 2016; Beik et al. 2021) and image-guided therapy (Sherwood et al. 2017; Sun et al. 2018). However, the major drawback of relatively low sensitivity in MRI entails the use of contrast agents (CAs) (Lee et al. 2007). Currently, CAs are employed in 40–50% cases of clinical MRI applications with the aim to improve sensitivity, especially for tumor diagnosis (Han et al. 2017; Cassidy et al. 2013; Wahsner et al. 2018).

There are two types of MRI CAs including T_1-weighted CAs generating a hyperintense signal known as positive CAs, and T_2-weighted negative CAs with a hypointense signal. Two parameters are considered for characterizing the function of MRI CAs, including longitudinal relaxivity (r_1) and relaxivity ratio defined as transverse relaxivity (r_2) divided by r_1 (r_2/r_1). The r_1 value implies the signal enhancement possibility of a CA, whereas the r_2/r_1 ratio shows the suitability of a CA to be used for T_1 or T_2-weighted MRI. In general, T_1-weighted CAs have low r_2/r_1 ratio (< 2) while T_2-weighted CAs have a larger r_2/r_1 ratio (> 10) (Tromsdorf et al. 2007).

Currently, gadolinium-based contrast agents (GdCAs) and superparamagnetic iron oxide (SPIO) nanoparticles are the most frequently used T_1 and T_2-weighted MRI CAs, respectively (Li et al. 2013; Gao et al. 2016). However, GdCAs have serious shortcomings that hamper their extensive prescription. They have a short circulation half-life and are rapidly excreted through the kidney that limits the precise diagnosis and prevents long-term monitoring (Kim et al. 2011; Caravan 2006). A number of studies reported the suboptimal biological stability of GdCAs, leading to the accumulation of Gd (III) in central nervous system, bone and kidney. These safety concerns have led to restriction of the intravenous use of linear GdCAs (Magnevist or Omniscan) by the European Medicines Agency (EMA) and a "black-box warning" on GdCAs by the US Food and Drug Administration (FDA) (Wahsner et al. 2018; Dekkers et al. 2018). Furthermore, present GdCAs have low longitudinal relaxivity value around 4 $mM^{-1}S^{-1}$ (Zhou and Lu 2013; Zhang et al. 2018). These emphasize the need for an ideal stable and biocompatible T_1-weighted CA with high r_1 value and low r_2/r_1 ratio.

Iron oxide nanoparticles are highly biocompatible and their magnetic properties are strongly size dependent. The magnetic moment of iron oxide NPs reduces by decreasing their size because of the reduction of their volume magnetic anisotropy and spin-canting effect on the surface of the particles (Kim et al. 2011). Accordingly, ultrasmall iron oxide NPs (US-IO) with sizes < 5 nm have been introduced as a potential T_1-weighted MRI CAs. However, recent studies suggested that the low r_1 value and not sufficiently low r_2/r_1 ratio prevent US-IO to compete with GdCAs in terms of image contrast enhancement (Shen et al. 2017; Li et al. 2019). Thus far, a number of studies have begun to explore the benefits of hybridizing US-IO with GdCAs with the aim to increase relaxivity, which in turn allows T_1-weighted MRI CAs to be administered at lower Gd dosage. However, recent efforts have been mostly unable to develop an optimized CA with sufficiently high r_1 value and low r_2/r_1 ratio at the same time. In this study, we proposed a wet-chemical synthesis technique to form a nanocomposite consisting of US-IO and Gd_2O_3 hybrid nanoparticles (FG-HNPs) stabilized with dextran, and investigated their potential for T_1-weighted MR imaging of colorectal adenocarcinoma tumor cells in vitro and in vivo. Scheme 1 shows the overall steps for the synthesis of this hybrid nanostructure.

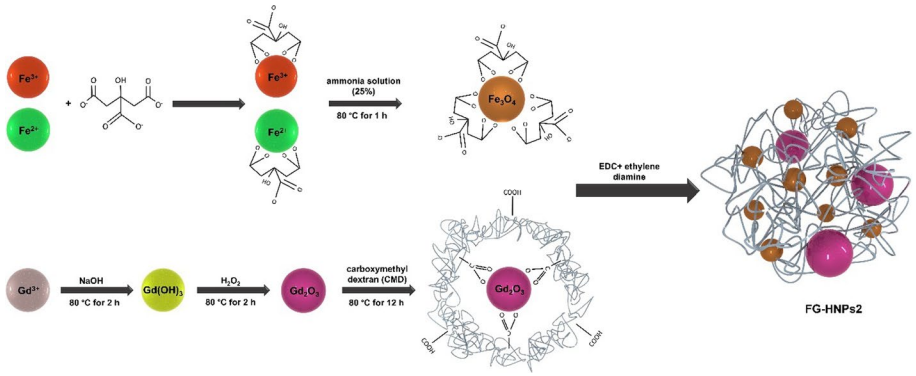

Scheme 1 Schematic for synthesis steps of FG-HNPs2 with high r_1 value and low relaxivity ratio (r_2/r_1) for T_1-weighted MRI

Materials and methods

Materials

Fetal bovine serum (FBS) was purchased from Gibco® (USA). Roswell Park Memorial Institute (RPMI) 1640 cell culture medium, penicillin–streptomycin and trypsin-ethylene diamine tetra acetic acid (EDTA) were purchased from the Sigma-Aldrich Company (USA). All mentioned materials were used for cell culture experiment. Iron (III) chloride ($FeCl_3$, ≥ 97%), iron (II) sulfate heptahydrate ($FeSO_4{\cdot}7H_2O$), sodium citrate, ammonia 25%, dextran 10 kDa (Mw = 1500), bromoacetic acid, sodium hydroxide (NaOH) (> 99.9%), ethanol, sodium borohydride, HCl, gadolinium nitrate, diethylene glycol, glycine and H_2O_2 were purchased from Sigma-Aldrich and used for synthesis of the nanocomposite.

Synthesis of US-IO

Firstly, 6 mmol citric acid was dissolved in 50 mL deionized water using magnetic stirring at room temperature. Then, 4 mmol $FeCl_3$ and 2 mmol $FeCl_2$ were dissolved in 50 mL deionized water and mixed into the solution, followed by dropwise adding 3 mL of ammonia solution (25%). The mixture was moderately stirred at 80 °C for 1 h. The obtained solution was then purified through dialysis to remove the unreacted and residual ions from the product.

Synthesis of Gd_2O_3@CMD and Gd_2O_3@Gly

Briefly, 1 mmol of $GdCl_3{\cdot}xH_2O$ was dissolved in 20 mL triethylene glycol in a three-necked flask using magnetic stirring at 40 °C. 3 mmol of NaOH was also added to 10 mL triethylene glycol in a separate container and then stirred at 40 °C. The NaOH solution was added to the Gd solution and the resulting mixture was stirred at 80 °C for 2 h, followed by adding 3.5 mL H_2O_2 to the reaction solution and continued stirring for another 2 h. Next, 0.1 mmol carboxymethyl dextran (CMD) or glycine (Gly) were added to the obtained solution while stirring at 80 °C for 12 h. The resulting products were dried at room temperature and dispersed in 400 mL ethanol and then washed 3 times through centrifugation at 12,000 rpm to remove unreacted precursors,

free ligands and solvent. Finally, the synthesized Gd_2O_3@CMD and Gd_2O_3@Gly were repeatedly washed with deionize water and prepared for further analyses.

Synthesis of FG-HNPs

To synthesize the final hybrid nanoparticles, the above products of citrate-capped Fe_3O_4 NPs (250 µL, 2 mg/mL) and Gd_2O_3@CMD (250 µL, 2.8 mg/mL) were mixed. Next, carboxylic groups on the surface of Fe_3O_4 and Gd_2O_3 were activated by adding 0.25 mg 1-Ethyl-3-(3 dimethylaminopropyl) carbodiimide hydrochloride (EDC), and then 65 µL of ethylene diamine were dropwise added to the solution under vigorous stirring. The resulting mixture was stirred at room temperature with pH between 6 and 7 for 1 h. To purify the final product, the sample was washed three times through centrifugation at 3000 rpm for 15 min and then dried in an oven at 80 °C for 3 h. FG-HNPs of different Gd/Fe molar ratio (0.25–3) were obtained and name as FG-HNPs1-5.

Characterizations

Transmission electron microscopy imaging (TEM) was performed through a LEO 906; ZEISS microscope at an accelerating voltage of 120 kV. Samples were prepared by depositing a dilute particle suspension (5 µL) onto a carbon coated copper grid and air-dried before analysis. The concentration of Fe and Gd in the samples was measured by inductively coupled plasma optical emission spectrometry (ICP-OES) (Varian 730-ES). Dynamic light scattering (DLS) and zeta potential measurements were conducted using Particle Metrix, NANO-flex system equipped with a He/Ne laser of 633 nm wavelength. Low angle X-ray diffraction (XRD) analysis was obtained from a PW1730-Philips system with KCu (1.54 Å) radiation. Fourier transform infrared (FTIR) spectra were collected on a Frontier infrared spectrophotometer (PerkinElmer). The chemical composition of the synthesized nanocomposite was determined using energy dispersive X-ray spectroscopy (EDS, MIRA II, FESEM, TESCAN).

Cell culture

Mouse colon adenocarcinoma CT26 cell line was obtained from Pasteur Institute of Iran. Cells were cultured as monolayers in RPMI 1640 medium supplemented with 10% FBS, 100 units/mL penicillin, and 100 µg/mL streptomycin. Cells were incubated in a humidified atmosphere containing 5% of CO_2 at 37 °C. To harvest cells, they were trypsinized with 1 mM EDTA/0.25% trypsin (*w*/*v*) in PBS.

Cytotoxicity assay

The cytotoxicity of the nanocomposite was assessed by using the methyl thiazolyl tetrazolium (MTT) method. Firstly, 100 µL of CT26 cell suspensions at a concentration of 5×10^4 cells/mL in complete RPMI medium were seeded into 96-well plate and allowed to adhere for 24 h. The medium was replaced with a fresh one containing FG-HNPs2, or Dotarem at varying Gd concentrations. After 4, 12 and 24 h incubation at 37 ℃, 50 µL of MTT (1.0 mg/mL in PBS) was added to each well. The medium was then removed after an additional 4 h of incubation, followed by adding 100 µL of dimethyl sulfoxide (DMSO) to each well to dissolve the formed formazan crystals. The absorbance was measured at 570 nm using a Bio-Rad ELISA reader.

MRI relaxometry

For MRI phantom study, sample solutions (US-IO, Gd_2O_3@Gly, Gd_2O_3@CMD, FG-HNPs1-5 and Dotarem) with various concentrations were prepared and scanned with a volumetric coil using two clinical MRI scanner systems (3 T, Magnetom Prisma, Siemens, Germany; 1.5 T, Magnetom Avanto, Siemens, Germany). The r_1 values were obtained by analysis of the MR images at different repetition time (TR) values (5000, 3000, 1800, 1200, 600, 300, 100 ms) and the constant echo time (TE) value of 12 ms using ImageJ and MATLAB. Likewise, the r_2 values were obtained from MR images at different TE values (12, 24, 36, 48, 60, 72, 84, 96, 108, 120, 132, 144, 156, 168 ms) and the constant TR value of 2000 ms.

In vitro *MRI study*

Firstly, the performance of FG-HNPs2 to sever as T_1-weighted MRI CAs was compared with US-IO and Dotarem on cancer cells in vitro. Typically, 2 mL of CT26 cell suspensions at a density of 1.0×10^5 cells/mL in complete growth medium were seeded into 6-well plate. After cell adherence, cells were incubated with Dotarem, US-IO and FG-HNPs2 at the same Gd and Fe concentration range (5, 10, 25, 50, and 100 μg/mL) for 4 h. Cells were then twice washed with PBS, trypsinized, and then centrifuged at 500 × g for 5 min to remove unloaded particles. The obtained cells were resuspended in 0.2 mL agarose solution (1%) in 2-mL Eppendorf tubes. The samples were placed in a 4 °C refrigerator until solidification, and then used for imaging by MRI scanner (1.5 and 3.0T, TE = 14 ms, TR = 800 ms, flip angle = 120, slice thickness = 0.7 mm, average = 10).

Tumor induction

BALB/c mice (5–8 weeks old, 20–25 g) were obtained from Pasteur Institute of Iran and housed in an isolated animal room under standard environmental conditions. All animal procedures were conducted in accordance with the guidelines for animal experimentation established by Iran University of Medical Sciences. Tumor induction was performed through subcutaneous injection of 2×10^6 CT26 cells suspended in 200 μL RPMI 1640 solution into the right flank of BALB/c mice. The tumor dimensions were measured via a caliper at predetermined times and the tumor volume was calculated as $a.b^2/2$, where a and b are the length and width of the tumor, respectively.

In vivo *MRI study*

The in vivo MRI experiment was performed on Siemens (3T, Magnetom Prisma, Siemens, Germany) MRI scanner system using a rat coil. Firstly, tumor-bearing mice were anesthetized via an intraperitoneally (i.p.) injection of 100 mg/kg ketamine and 10 mg/kg xylazine. Mice were kept warm by circulating warm water (37 ℃) and placed in a stretched prone position. T_1-weighted images were acquired at pre-injection and post i.v. injection of Dotarem (5 mg/kg per Gd), FG-HNPs2 (5 mg/kg per Gd) and US-IO (5 mg/kg per Fe). The image acquisition was conducted using a T_1 sequence with the following parameters: TR = 800 ms, TE = 14 ms, flip angle = 120°, matrix size = 256 × 256, slices = 14, slice thickness = 0.7 mm. Signal-to-noise ratio (SNR)

was obtained by analyzing regions of interest (ROIs) by measuring signal intensity through Image J software. SNR and ΔSNR (i.e., signal enhancement) were calculated according to Eqs. (1) and (2):

$$\mathrm{SNR} = \mathrm{SI}_{\mathrm{mean}}/\mathrm{SD}_{\mathrm{noise}}, \tag{1}$$

$$\Delta\mathrm{SNR} = (\mathrm{SNR}_{\mathrm{post}} - \mathrm{SNR}_{\mathrm{pre}})/\mathrm{SNR}_{\mathrm{pre}} \times 100\%, \tag{2}$$

where SI_{mean} is the mean T_1 signal intensity and SD is the standard deviation of the background signal.

In vivo *biodistribution*

Biodistribution study was performed by using ICP-OES to determine the optimum time after injection for maximal tumor accumulation of FG-HNPs2. To this end, tumor-bearing mice were sacrificed at 6, 24 h and 6 days post-injection of Dotarem or FG-HNPs2 (5 mg/kg per Gd). The tumor and major organs (heart, liver, spleen, lung, kidney and brain) were extracted and weighed. The organs were cut into 1–2 mm^2 pieces and digested by aqua regia solution ($HCl:HNO_3 = 3:1$) for 24 h. Then, the Gd content of different organs was quantified by ICP-OES. To draw a comparison, the mice without injection were used as control.

Histological examination

The histological analysis was performed following standard procedures. CT26 tumor-bearing mice were injected with FG-HNPs2 and US-IO at the same dose of 5 mg/kg. The tumor and major organs were extracted and fixed overnight in 10% neutral-buffered formalin, embedded in paraffin blocks, cut into 5-μm sections, and mounted onto glass slides. After hematoxylin and eosin (H&E) staining, the histological changes were investigated under an optical microscope (Primo Star, ZEISS). Prussian blue (PB) staining was performed to investigate the tumor localization of the magnetic particles. 5-μm-thick tissue sections were prepared as described above, and then incubated with PB staining solution containing equal parts of 5% HCl and 5% potassium ferrocyanide for 30 min, followed by counterstaining with nuclear fast red. Furthermore, tumor tissue was studied by TEM to investigate the tumor cell uptake of the particles. To this end, the tumor was fixed in 2.5% glutaraldehyde and prepared for TEM examination as reported in our previous study (Alamzadeh et al. 2019). Thin sections of tumor tissue were transferred on the 200-mesh uncoated grids and underwent TEM observation (LEO 906; Zeiss) at the acceleration voltage of 120 kV.

Statistical analysis

For statistical analysis, one-way ANOVA was performed using SPSS (version 11; SPSS Inc., Chicago, IL). All data are expressed as the mean ± standard deviation (SD). A value of $p < 0.05$ was considered to be statistically significant.

Results and discussion

Characterization

The morphology and size distributions analysis of the particles by TEM (Fig. 1a) and DLS (Fig. 1b) showed that US-IO and FG-HNPs2 are spherical, fairly uniform

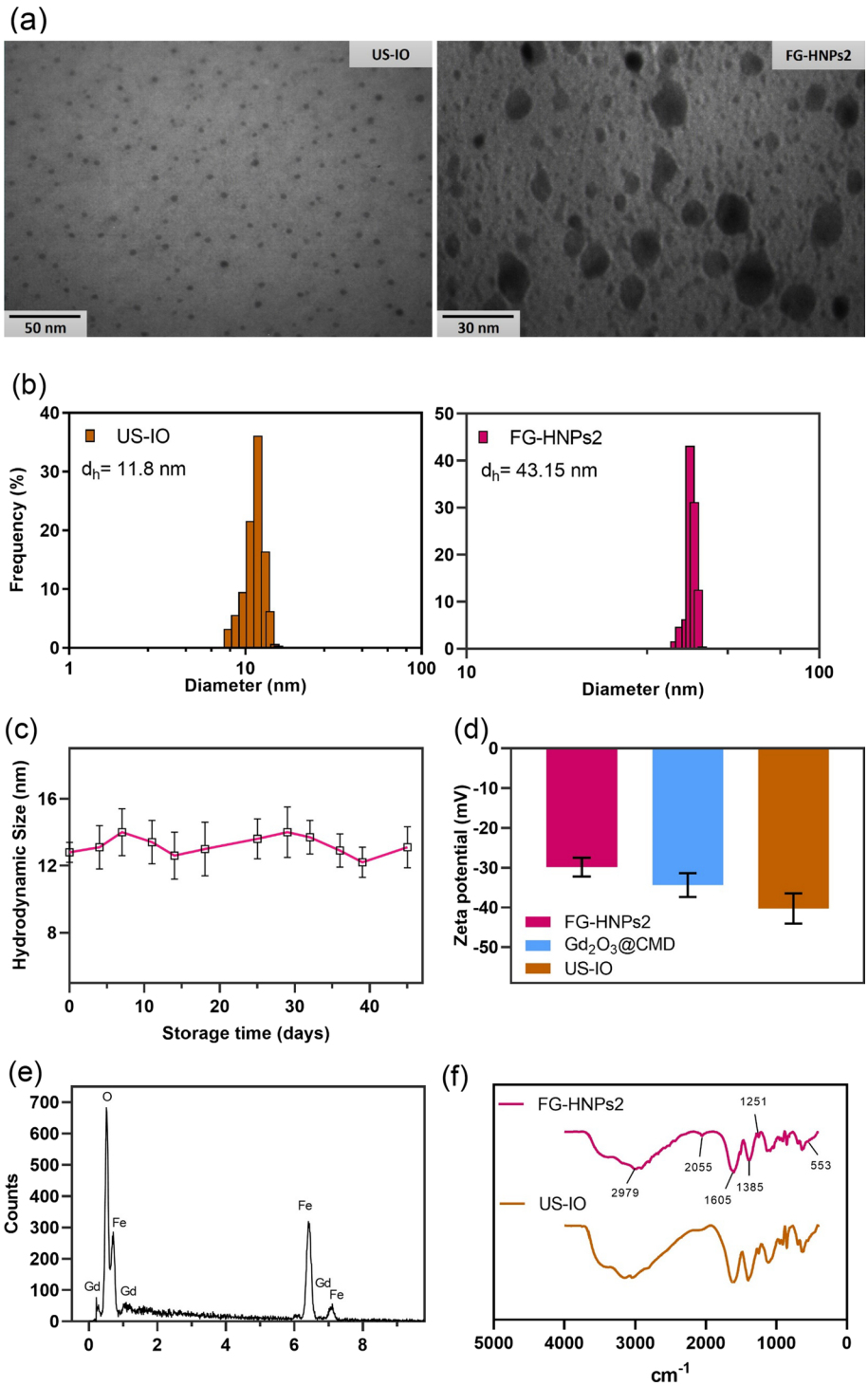

Fig. 1 Characterization of FG-HNPs2. **a** TEM images of US-IO and FG-HNPs2. **b** Hydrodynamic diameter (d_h) of US-IO and FG-HNPs2 measured by DLS. **c** Hydrodynamic diameter (d_h) changes of FG-HNPs2 (C_{Gd} = 1.0 mM) during storage at 4 ℃ (mean ± SD, n = 3). **d** Zeta potential measurement of FG-HNPs2, Gd_2O_3@CMD, US-IO (pH = 7.1). **e** Energy dispersive X-ray spectra (EDS) of FG-HNPs2. **f** FTIR spectra of the FG-HNPs2 and US-IO

in shape and size and well-dispersed without aggregation. The mean particle size for US-IO and FG-HNPs2 was measured to be 3.78 ± 0.2 and 13.86 ± 0.36 nm by TEM (Additional file 1: Fig. S1). The hydrodynamic diameter (d_h) of US-IO measured by DLS was found to be 11.8 nm, whereas FG-HNPs vary in d_h from 39.11 to 51.16 nm by increasing Gd/Fe molar ratio from 0.25 to 3 (Table 1). The colloidal stability of FG-HNPs2 was also confirmed by measuring the d_h changes during storage for up to 45 days at 4 °C (Fig. 1c). The Zeta potential (Fig. 1d) was measured to be − 40.28, − 34.38 and − 24.87 mV for US-IO, Gd_2O_3@CMD and FG-HNPs2, respectively, further indicating that the particles are highly stable in aqueous solution. The negative surface charge of the particles reduces their non-specific uptake by most of normal cells during circulation (Shen et al. 2019). The EDS (Fig. 1e) represents the characteristic peaks showing FG-HNPs2 consisting of Fe, Gd and O elements. The FTIR spectra (Fig. 1f) of FG-HNPs2 shows absorption peaks at 2979, 2055, 1385 and 1251 cm^{-1}, which can be ascribed to C–H stretching vibration, carbodiimide bond, C–H bending and C–O stretching vibrations, respectively. The peak at 1605 cm^{-1} refers to the asymmetric carbonyl group of carboxylates and the peak at 553 cm^{-1} is attributed to the Fe–O stretching vibration that are the characteristic bond vibrations for FG-HNPs2 components. The XRD pattern shows the crystalline structure of the samples in each synthetic step, which are consistent with the reference (JCPDS No. 98-001-7261 and 01-088-2165) (Additional file 1: Fig. S2). The peaks at 35.4°, 57.38° and 63.43° are ascribed to Fe_3O_4, and Gd_2O_3 displayed diffraction peaks at 2θ values of 28.4°, 33° and 47.58°.

Table 1 The r_1 and r_2 values of different samples under different magnetic fields

Sample nomenclature	H_0 (T) [a]	d_h (nm) [b]	Gd/Fe [c]	r_1 ($mM^{-1}S^{-1}$)	r_2 ($mM^{-1}S^{-1}$)	r_2/r_1
US-IO	3	11.8	–	0.512	2.1797	4.257
	1.5	11.8	–	0.3822	1.7985	4.706
Gd_2O_3@Gly	3	15.48	–	9.9529	48.852	4.908
	1.5	15.48	–	24.838	117.22	4.719
Gd_2O_3@CMD	3	28.12	–	10.351	41.752	4.034
	1.5	28.12	–	12.365	50.555	4.089
FG-HNPs1	3	39.11	0.25	2.9719	18.719	6.299
	1.5	39.11	0.25	8.6222	100.12	11.612
FG-HNPs2	3	43.15	0.5	42.28 ± 1.87	59.86 ± 2.53	1.416 ± 0.01
	1.5	43.15	0.5	43.55 ± 1.85	58.68 ± 1.54	1.35 ± 0.1
FG-HNPs3	3	45.6	1.0	28.155	41.714	1.482
	1.5	45.6	1.0	35.173	50.301	1.43
FG-HNPs4	3	49.72	2.0	24.412	38.864	1.592
	1.5	49.72	2.0	25.209	41.317	1.639
FG-HNPs5	3	51.16	3.0	8.8134	137.04	15.549
	1.5	51.16	3.0	24.158	141.36	5.851
Dotarem	3	–	–	3.12 ± 0.7	3.98 ± 0.21	1.278 ± 0.1
	1.5	–	–	2.96 ± 0.1	4.77 ± 0.14	1.61 ± 0.02

[a] Magnetic field of MRI scanner system

[b] Hydrodynamic diameter (d_h) determined by DLS

[c] Molar ratio of Gd to Fe

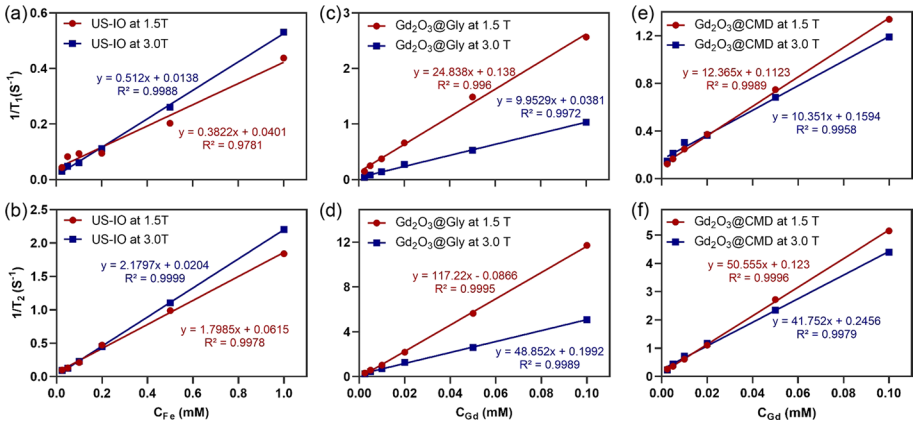

Fig. 2 **a**, **b** T_1 relaxation rate ($1/T_1$, s^{-1}) and T_2 relaxation rate ($1/T_2$, s^{-1}) plotted as a function of C_{Fe} for US-IO. **c**, **d** T_1 and T_2 relaxation rate plotted as a function of C_{Gd} for Gd_2O_3@Gly. **e**, **f** T_1 and T_2 relaxation rate plotted as a function of C_{Gd} for Gd_2O_3@CMD. T_1 relaxation rate: TE = 12 ms, TR = 100–5000 ms. T_2 relaxation rate: TE = 12–168 ms, TR = 2000 ms. The magnetic field was 1.5T or 3.0T

Relaxometry

The r_1 and r_2 values were measured for various synthetic formulations including US-IO, Gd_2O_3@Gly and Gd_2O_3@CMD through 1.5 and 3.0 T MRI scanner systems (Fig. 2). As summarized in Table 1, under 3.0 T MRI the r_1 value was calculated to be 0.51, 9.95 and 10.35 mM^{-1} s^{-1} for US-IO, Gd_2O_3@Gly and Gd_2O_3@CMD, respectively. The r_2/r_1 ratio was also calculated to be 4.26, 4.9 and 4.03 for US-IO, Gd_2O_3@Gly and Gd_2O_3@CMD, respectively. Accordingly, Gd_2O_3@CMD with higher r_1 value and lower r_2/r_1 ratio compared to Gd_2O_3@Gly was used in our final nanocomposite formula.

Figure 3a shows black/white and colored T_1-weighted MR images of FG-HNPs solutions with varying Gd/Fe molar ratio at 3.0 T. Apparently, FG-HNPs2 reveals higher brightness than FG-HNPs1, 3, 4, 5 at given C_{Gd} because of the higher r_1 value and lower r_2/r_1 ratio as measured in Fig. 3b and c. The changes in r_1 value and r_2/r_1 ratio as a function of Gd/Fe molar ratio (Fig. 3d) indicates that the increase in Gd/Fe molar ratio from 0.25 to 0.5 dramatically increases the r_1 value from 2.97 to 42.63 mM^{-1} s^{-1}, and decreases the r_2/r_1 from 6.3 to 1.41. Therefore, the higher Gd content of FG-HNPs2 compared to FG-HNPs1 results in stronger T_1-weighted contrast enhancement. On the other hand, FG-HNPs2 with smaller size and larger surface-to-volume ratio could outperform FG-HNPs3-5 because of the presence of more naked metal on their surface to interact with the proton of H_2O, leading to higher r_1 value (Shen et al. 2017). According to Eq. 3, the r_1 value of FG-HNPs2 is higher than FG-HNPs3-5, where q^{ss} is the number of bounded water molecules, P_m is the mole fraction of water coordinated to the Gd center, T_{1m} is T_1 relaxation time and τ_M is the residency time of water molecules in the second-sphere (Shen et al. 2018):

$$\frac{1}{T_1} = \frac{q^{ss} P_m}{T_{1m} + \tau_M}. \tag{3}$$

The SNR and ΔSNR were also calculated for quantification of MR images according to Eqs. (1) and (2). As shown in Fig. 3e, under the same C_{Gd}, FG-HNPs2 indicated a higher ΔSNR compared to other formulations, further certifying the superior performance of

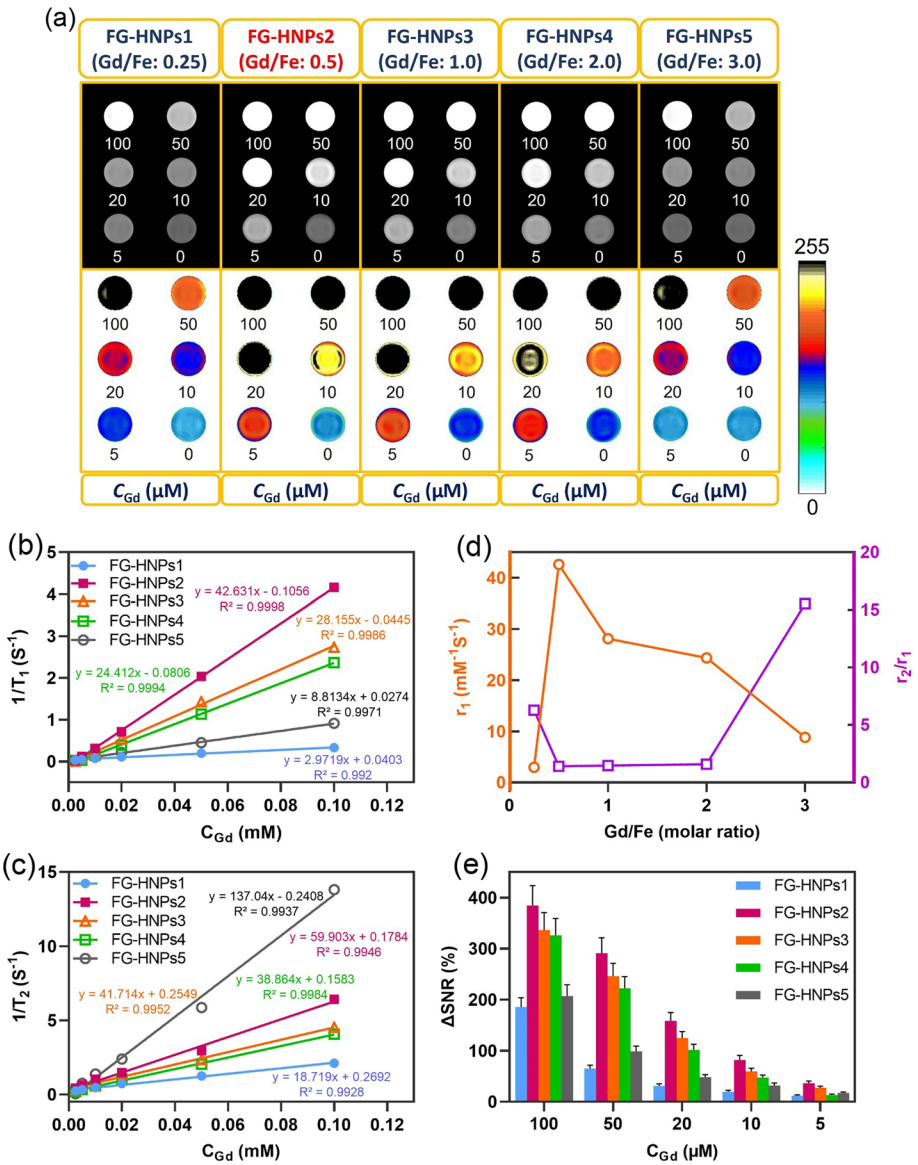

Fig. 3 **a** T_1-weighted MR images of FG-HNPs with 0.25–3 Gd/Fe molar ratios at varying Gd concentrations (TE = 12 ms, TR = 600 ms). **b** T_1 and **c** T_2 relaxation rates plotted as a function of C_{Gd} for FG-HNPs1-5. T_1 relaxation rate: TE = 12 ms, TR = 100–5000 ms. T_2 relaxation rate: TE = 12–168 ms, TR = 2000 ms. **d** r_1 value or r_2/r_1 ratio plotted as a function of Gd/Fe molar ratio. **e** ΔSNR of the MR images for FG-HNPs1-5 at various Gd concentrations measured by ImageJ software compared to pure water ($C_{Gd} = 0$). The magnetic field was 3.0T

FG-HNPs2 as T_1-weighted CAs. Since the r_1 and r_2 values highly rely on the applied magnetic field, similar experiments were conducted under 1.5T MRI scanner system (Additional file 1: Fig. S3). Taken together, according to the results of MRI relaxometry the Gd/Fe molar ratio for our nanoprobe structure was optimized to be 0.5, so as to offer a higher r_1 value and a lower r_2/r_1 ratio (Wahsner et al. 2018; Warsi et al. 2010). Interestingly, the obtained r_2/r_1 ratio for FG-HNPs2 is comparable to that of Dotarem and lower than mostly reported T_1-weighted MRI CAs (Qin et al. 2020; Yang et al. 2011; Perrier et al. 2015; Li et al. 2016; Zhou et al. 2015). Therefore, FG-HNPs2 can be suggested as promising T_1-weighted MRI CAs by virtue of notably high r_1 value and low

r_2/r_1 ratio. Additional file 1: Figs. S4 and S5 show the results of relaxometry for three different batches of FG-HNPs2 and Dotarem at 1.5 and 3.0T. Additional file 1: Fig. S6 also shows the plot of T_1 signal intensity versus TR for three different batches of FG-HNPs2 at various $C_{Gd,}$ showing that where the T_1 signal intensity is saturated at any given concentration.

Cytotoxicity assay

The cytocompatibility of FG-HNPs2 was evaluated by MTT assay and compared with commercially available Dotarem. Figure 4 shows the viability of CT26 cells exposed to FG-HNPs2 and Dotarem at varying concentrations (0.02–2 mM) for 4 h, 12 h and 24 h. Obviously, CT26 cells indicated a gradual decrease in cell viability with increasing C_{Gd}. However, under the same C_{Gd}, the viability of cells treated with FG-HNPs2 remained significantly higher than those treated with Dotarem. The higher cytocompatibility of FG-HNPs2 can be due to the lower toxic effect of Gd_2O_3 in comparison to Gd ions in Dotarem, as well as the presence of dextran coating that stabilizes $Gd_2O_{3.}$ Therefore, the as-prepared FG-HNPs2 displayed a good cytocompatibility to be used for biomedical applications.

In vitro T_1-weighted MR imaging

Next, we explored the potential of FG-HNPs2 to serve as T_1-weighted MRI CAs for imaging of cancer cells in vitro. It can be visualized from 3.0T MR images of cancer cells in Fig. 5a that FG-HNPs2 yielded a clearly brighter contrast compared to US-IO and Dotarem at the same C_{Gd} or C_{Fe}. The quantification of MR signal intensity (Fig. 5b) further proved that cells treated with FG-HNPs2 exhibit a significantly higher ΔSNR as compared to US-IO- and Dotarem-treated cells ($p < 0.05$). Similar results were obtained for T_1-weighted MR imaging of cancer cells under 1.5T MRI scanner system (Additional file 1: Fig. S7).

In vivo T_1-weighted MR imaging

Inspired by the in vitro results, the potential of FG-HNPs2 to be used as tumor imaging probes was explored in vivo. To this end, CT26 tumor-bearing mice were i.v. injected with Dotarem, US-IO, and FG-HNPs2 (5.0 mg/kg per Gd or Fe) and MR images were acquired at various times post-injection (Fig. 6). As shown in Fig. 6a, the brightness of MR images was noticeably enhanced with a time-dependent manner in all injection groups compared to untreated control. Following the injection of Dotarem, US-IO and

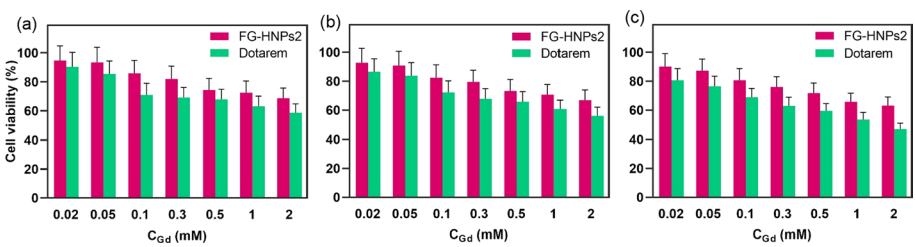

Fig. 4 Viability of CT26 cells treated with FG-HNPs2 and Dotarem® at varying Gd concentrations for **a** 4 h, **b** 12 h and **c** 24 h. Mean ± SD, $n = 4$

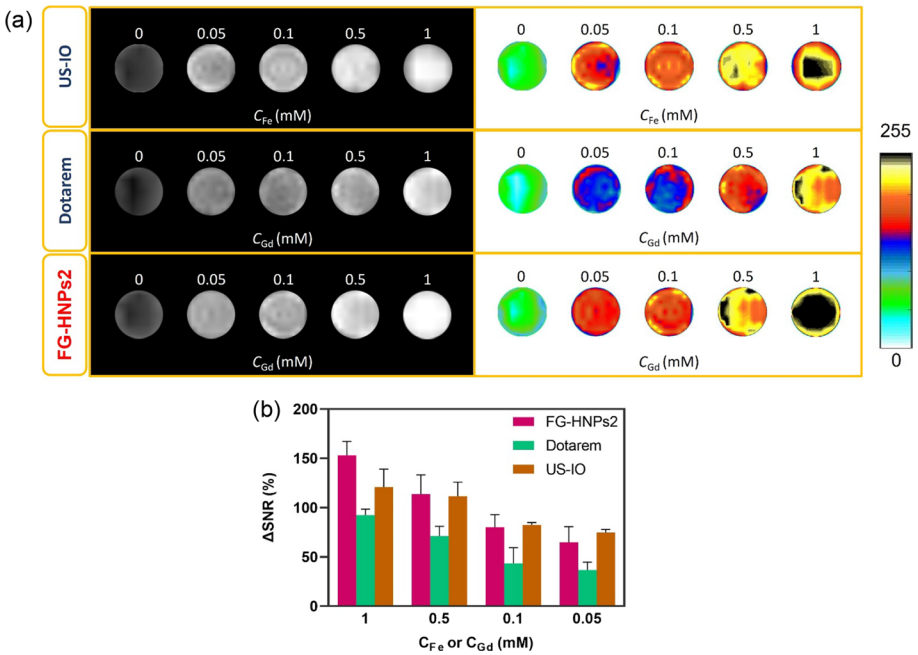

Fig. 5 **a** T_1-weighted MR images of CT26 cells exposed with US-IO, Dotarem® and FG-HNPs2 at varying Fe or Gd concentrations. TR = 800 ms, TE = 14 ms. **b** ΔSNR of MR images of cancer cells for US-IO, Dotarem® and FG-HNPs2 groups compared to the control (C_{Fe} or C_{Gd} = 0). Mean ± SD, n = 3. The magnetic field was 3.0T

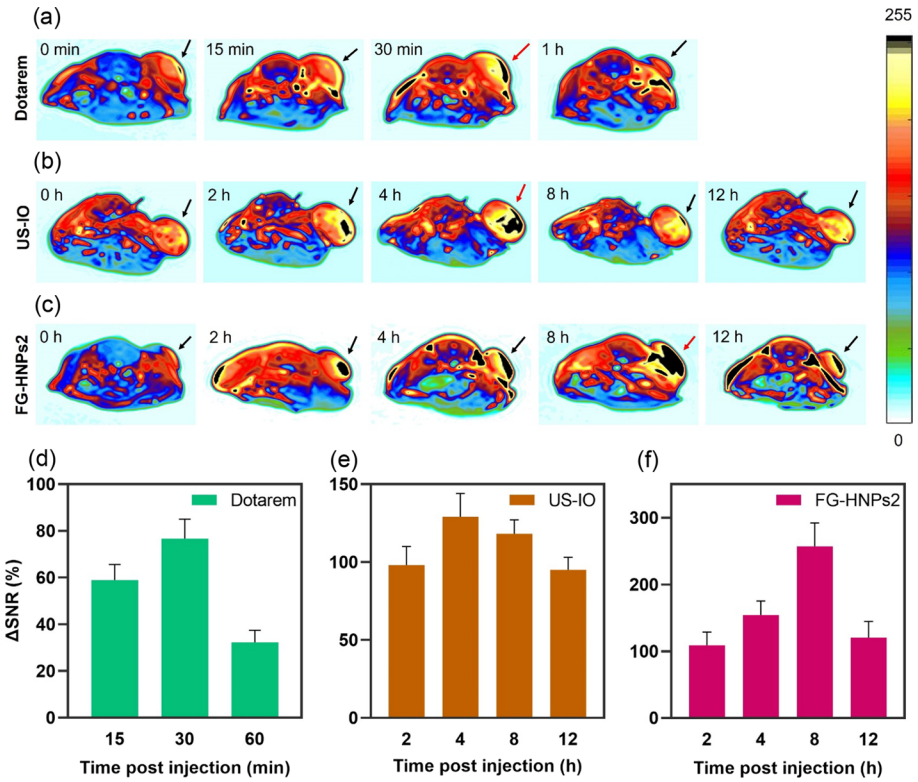

Fig. 6 **a**–**c** In vivo T_1-weighted MR images of CT26 tumor-bearing mice (slice orientation: axial) at different times post-injection of Dotarem® (C_{Gd} = 5.0 mg/kg), US-IO (C_{Fe} = 5.0 mg/kg) and FG-HNPs2 (C_{Gd} = 5.0 mg/kg). TR = 800 ms, TE = 14 ms. **d**–**f** Quantitative analysis of the tumor region after injection of Dotarem®, US-IO and FG-HNPs2 by ΔSNR. The magnetic field was 3.0T

FG-HNPs2, the MR signal intensity of the tumor region reached its maximum level at different time points of 30 min, 4 h and 8 h, respectively, which could be attributed to the difference in the size of the particles. Due to their larger size, US-IO ($d_h = 11.8$ nm) and FG-HNPs2 ($d_h = 43.15$ nm) have a longer circulation lifetime than the small molecule Dotarem ($M_w = 753.9$) which can be quickly removed from the body through the kidney. More importantly, the tumor treated with FG-HNPs2 showed a markedly stronger contrast enhancement, quantified by ΔSNR, at the peak time (257.025 ± 17.4% at 8 h post-injection) when compared to Dotarem (76.71 ± 14.2% at 30 min post-injection) and US-IO (129.102 ± 15% at 4 h post-injection) (Fig. 6d–f). These results suggest that the as-prepared FG-HNPs2 have a superior T_1 contrast enhancement effect than the routinely used Dotarem and are comparable to the best previously reported T_1-weighted CAs (Shen et al. 2017; Li et al. 2019, 2016; Qin et al. 2020; Yang et al. 2011; Perrier et al. 2015; Zhou et al. 2015).

In vivo *biodistribution*

We further investigated the biodistribution of FG-HNPs2 in tumor-bearing mice via the measurement of Gd element by ICP-OES. Figure 7a shows the Gd content of the tumor and healthy organs in mice at 1 h post-injection of Dotarem and 24 h post-injection of FG-HNPs2 (5.0 mg/kg per Gd) as compared to untreated control. The maximum concentration of Gd in the tumor treated with FG-HNPs2 was found to be nearly 4.67-fold higher than that treated with Dotarem. The way of accumulation of Dotarem and FG-HNPs2 in body organs further proved that while Dotarem

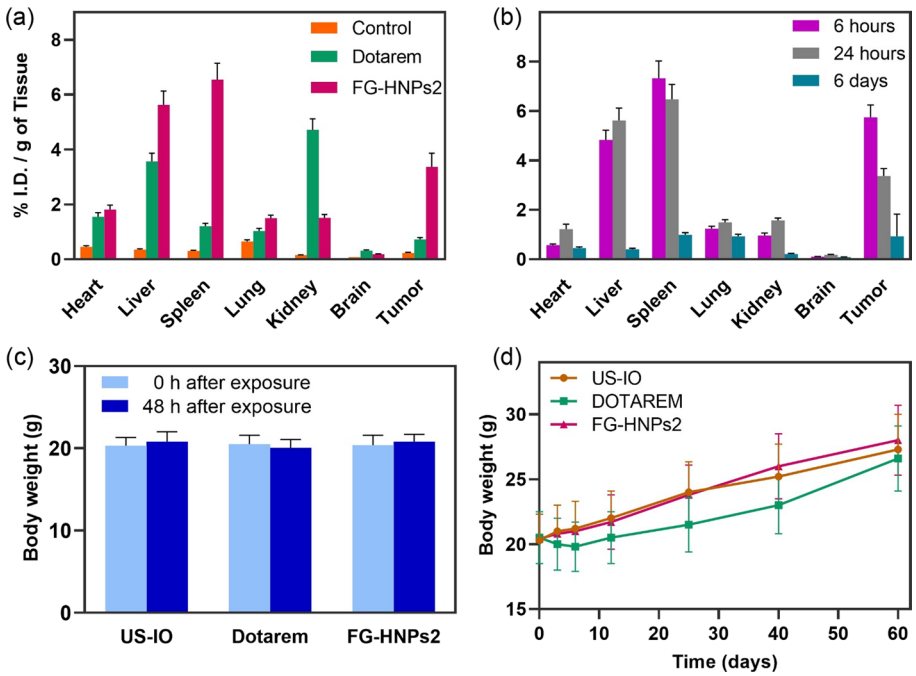

Fig. 7 **a** The biodistribution of Gd element in the tumor and major organs at 1 h post-injection of Dotarem and 24 h post-injection of FG-HNPs2. **b** The biodistribution of Gd element in CT26 tumor-bearing mice at 6 h, 24 h or 6 days post-injection of FG-HNPs2 (Gd dosage = 5.0 mg/kg). **c**, **d** The body weight changes in CT26 tumor-bearing mice following various injections

is mainly washed out of the body through the kidney, FG-HNPs2 with the hydrodynamic size larger than the renal clearance threshold (~ 6 nm) are predominantly taken up by the reticuloendothelial system including liver and spleen. Figure 7b shows the difference in the Gd content of the tumor and other organs at various time points of 6 h, 24 h and 6 days following the injection of FG-HNPs2. The amount of Gd in all organs was found to be comparable to that of control group (< 1% ID per g of tissue) after 6 days post-injection, indicating that the injected FG-HNPs2 were completely removed from the body. Therefore, the risk of long-term toxicity to healthy organs due to the accumulation of Gd would not a matter of concern after FG-HNPs2 injection. The systemic toxicity of various agents was further evaluated by monitoring the body weight changes of animals for up to 60 days post-injection (Fig. 7c, d). While no reduction in body weight was observed for mice receiving US-IO and FG-HNPs2, Dotarem-injected group displayed a slight decrease in body weight during the first week of follow-up. Therefore, the as-prepared FG-HNPs2 are non-toxic and well-tolerated in vivo.

Histological studies

Figure 8A represents the result of histological analysis by H&E staining on major organs in CT26 tumor-bearing mice with or without FG-HNPs2 injection (5 mg/kg per Gd, 48 h post-injection). As compared to untreated control, the mice treated with FG-HNPs2 exhibited no obvious toxicity to major organs, further proving that FG-HNPs2 are highly biocompatible to serve as MRI CAs. The tumor uptake of FG-HNPs2 was further investigated by PB staining and TEM. PB staining of tumor tissue demonstrated the presence of iron-positive cells, confirming the efficient tumor localization of FG-HNPs2 following i.v. injection (Fig. 8b). Additionally, TEM micrograph of tumor tissue manifested the efficient penetration and retention of FG-HNPs2 in the tumor cells (Fig. 8c).

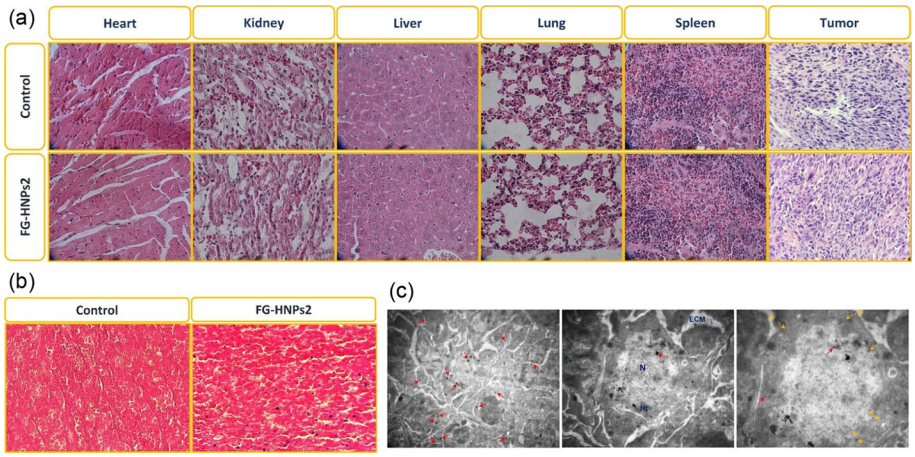

Fig. 8 **a** H&E staining of major organs collected from CT26 tumor-bearing mice with or without FG-HNPs2 injection after 48 h (C_{Gd} = 5.0 mg/kg). **b** Prussian blue (PB) stained-images of tumor tissue 24 h following i.v. injection of FG-HNPs2 (C_{Gd} = 5.0 mg/kg). **c** TEM images of tumor tissue after 24 h post-injection of FG-HNPs2 (C_{Gd} = 5.0 mg/kg)

Conclusion

In summary, we developed a convenient method to prepare novel FG-HNPs2 with high r_1 value (42.28 $mM^{-1}S^{-1}$) and low relaxivity ratio (r_2/r_1: 1.416), that represent superior image contrast enhancement than commercial Gd chelates and most of the reported T_1-weighted MRI contrast agents. Cell cytotoxicity assay and animal experiments proved that FG-HNPs2 are highly biocompatible without showing short- and long-term safety concerns. The biodistribution studies demonstrated the efficient tumor localization and retention of FG-HNPs2 after systemic injection. Finally, in vitro and in vivo T_1-weighted MR imaging showed that FG-HNPs2 could outperform the commercially available Dotarem in terms of generating bright signals. Therefore, this nanohybrid platform could appear a promising candidate to serve as a T_1-weighted MRI contrast agent.

Supplementary Information

The online version contains supplementary material available at https://doi.org/10.1186/s12645-022-00148-5.

Additional file 1: Fig. S1. Size distributions of (a): US-IO and (b): FG-HNPs2 measured from the TEM images. **Fig. S2.** XRD patterns of (a): Gd_2O_3, (b): US-IO, (c): Gd_2O_3 @CMD, (d): FG-HNPs2. FG-HNPs2 was heated in furnace to remove dextran coating (The dextran coating prevented to see the XRD pattern. To remove it, under nitrogen gas, 10 ˚C was added to the temperature every 1 minute to reach 900 ˚C). The peaks related to Gd_2O_3 and Fe_3O_4 are indicated by asterisks * and double asterisks **, respectively. **Fig. S3.** (a) T_1-weighted MR images of FG-HNPs with 0.25-3 Gd/Fe molar ratios at varying Gd concentrations (TE = 12 ms, TR = 600 ms). (b) T_1 and (c) T_2 relaxation rates plotted as a function of C_{Gd} for FG-HNPs1-5. T_1 relaxation rate: TE = 12 ms, TR = 100 ~ 5000 ms. T_2 relaxation rate: TE = 12 ~168 ms, TR = 2000 ms. (d) r_1 value or r_2/r_1 ratio plotted as a function of Gd/Fe molar ratio. (e) ΔSNR of the MR images for FG-HNPs1-5 at various Gd concentrations measured by ImageJ software compared to pure water (C_{Gd}=0). The magnetic field was 1.5 T. **Fig. S4.** (a, b): T_1 relaxation rate ($1/T_1$, s^{-1}) or T_2 relaxation rate ($1/T_2$, s^{-1}) plotted as a function of C_{Gd} for FG-HNPs2 prepared from 3 batches (*i.e.*, FG-HNPs2-1, FG-HNPs2-2, FG-HNPs2-3) were synthesized from 3 different batches at same conditions. (c, d): T_1 or T_2 relaxation rate plotted as a function of C_{Gd} for commercial Dotarem® prepared from 3 batches (*i.e.*, Dotarem-1, Dotarem-2, Dotarem-3). For T_1 relaxation rates: TE = 12 ms, TR = 100 ~ 4000 ms. For T_2 relaxation rates: TE = 12 ~168 ms, TR = 2000 ms. The magnetic field was 1.5 T. **Fig. S5.** (a, b): T_1 relaxation rate ($1/T_1$, s^{-1}) or T_2 relaxation rate ($1/T_2$, s^{-1}) plotted as a function of C_{Gd} for FG-HNPs2 prepared from 3 batches (*i.e.*, FG-HNPs2-1, FG-HNPs2-2, FG-HNPs2-3) were synthesized from 3 different batches at same conditions. (c, d): T_1 or T_2 relaxation rate plotted as a function of C_{Gd} for commercial Dotarem® prepared from 3 batches (*i.e.*, Dotarem-1, Dotarem-2, Dotarem-3). For T_1 relaxation rates: TE = 12 ms, TR = 100 ~ 4000 ms. For T_2 relaxation rates: TE = 12 ~168 ms, TR = 2000 ms. The magnetic field was 3.0 T. **Fig. S6.** (a-c) T_1 signal intensity versus TR values for three different batches of FG-HNPs2 at varying Gd concentrations. **Fig. S7.** (a) T_1-weighted MR images of CT26 cells exposed with US-IO, Dotarem® and FG-HNPs2 at varying Fe or Gd concentrations. TR = 800 ms, TE = 14 ms. (b) ΔSNR of MR images of cancer cells for US-IO, Dotarem® and FG-HNPs2 groups compared to the control (C_{Fe} or C_{Gd} = 0). Mean ± SD, n = 3. The magnetic field was 1.5 T.

Acknowledgements
Not applicable.

Author contributions
AS and MM performed animal experiments, ZA performed in vitro experiments, JB performed data analysis and drafted the manuscript, RI performed nanoparticle synthesis and characterization, VP performed TEM study, SKK provided scientific advice and edited the manuscript, HG and SK supervised the overall study design, analysis of data, and preparation of the manuscript. All authors read and approved the final manuscript.

Funding
This research was funded by Iran University of Medical Sciences (IUMS) (Grant No. 13462), and Zahedan University of Medical Sciences (ZUMS) (Grant No. 7970). The funders had no role in study design, data collection and analysis, decision to publish, or preparation of the manuscript.

Availability of data and materials
All data generated or analyzed during this study are included in this published article.

Declarations

Ethics approval and consent to participate
Not applicable.

Consent for publication
Not applicable.

Competing interests
The authors declare that they have no competing interests.

Received: 17 August 2022 Accepted: 28 November 2022
Published online: 09 December 2022

References

Alamzadeh Z, Beik J, Mahabadi VP, Ardekani AA, Ghader A, Kamrava SK et al (2019) Ultrastructural and optical characteristics of cancer cells treated by a nanotechnology based chemo-photothermal therapy method. J Photochem Photobiol, B 192:19–25
Ananta JS, Godin B, Sethi R, Moriggi L, Liu X, Serda RE et al (2010) Geometrical confinement of gadolinium-based contrast agents in nanoporous particles enhances T1 contrast. Nat Nanotechnol 5(11):815–821
Beik J, Alamzadeh Z, Mirrahimi M, Sarikhani A, Ardakani TS, Asadi M et al (2021) Multifunctional theranostic graphene oxide nanoflakes as MR imaging agents with enhanced photothermal and radiosensitizing properties. ACS Appl Bio Mater 4(5):4280–4291
Caravan P (2006) Strategies for increasing the sensitivity of gadolinium based MRI contrast agents. Chem Soc Rev 35(6):512–523
Cassidy M, Chan H, Ross B, Bhattacharya P, Marcus C (2013) In vivo magnetic resonance imaging of hyperpolarized silicon particles. Nat Nanotechnol 8(5):363–368
Dekkers IA, Roos R, van der Molen AJ (2018) Gadolinium retention after administration of contrast agents based on linear chelators and the recommendations of the European Medicines Agency. Eur Radiol 28(4):1579–1584
Fink C, Gaudet JM, Fox MS, Bhatt S, Viswanathan S, Smith M et al (2018) 19 F-perfluorocarbon-labeled human peripheral blood mononuclear cells can be detected in vivo using clinical MRI parameters in a therapeutic cell setting. Sci Rep 8(1):1–13
Gao Z, Ma T, Zhao E, Docter D, Yang W, Stauber RH et al (2016) Small is smarter: nano MRI contrast agents–advantages and recent achievements. Small 12(5):556–576
Han Z, Wu X, Roelle S, Chen C, Schiemann WP, Lu Z-R (2017) Targeted gadofullerene for sensitive magnetic resonance imaging and risk-stratification of breast cancer. Nat Commun 8(1):1–9
Huang G, Li H, Chen J, Zhao Z, Yang L, Chi X et al (2014) Tunable T1 and T2 contrast abilities of manganese-engineered iron oxide nanoparticles through size control. Nanoscale 6(17):10404–10412
Kim BH, Lee N, Kim H, An K, Park YI, Choi Y et al (2011) Large-scale synthesis of uniform and extremely small-sized iron oxide nanoparticles for high-resolution T1 magnetic resonance imaging contrast agents. J Am Chem Soc 133(32):12624–12631
Lee J-H, Huh Y-M, Jun Y-w, Seo J-w, Jang J-t, Song H-T et al (2007) Artificially engineered magnetic nanoparticles for ultra-sensitive molecular imaging. Nat Med 13(1):95–99
Li L, Jiang W, Luo K, Song H, Lan F, Wu Y et al (2013) Superparamagnetic iron oxide nanoparticles as MRI contrast agents for non-invasive stem cell labeling and tracking. Theranostics 3(8):595
Li F, Zhi D, Luo Y, Zhang J, Nan X, Zhang Y et al (2016) Core/shell Fe_3O_4/Gd_2O_3 nanocubes as T1–T2 dual modal MRI contrast agents. Nanoscale 8(25):12826–12833
Li F, Liang Z, Liu J, Sun J, Hu X, Zhao M et al (2019) Dynamically reversible iron oxide nanoparticle assemblies for targeted amplification of T1-weighted magnetic resonance imaging of tumors. Nano Lett 19(7):4213–4220
Liu K, Dong L, Xu Y, Yan X, Li F, Lu Y et al (2018) Stable gadolinium based nanoscale lyophilized injection for enhanced MR angiography with efficient renal clearance. Biomaterials 158:74–85
Mi P, Kokuryo D, Cabral H, Wu H, Terada Y, Saga T et al (2016) A pH-activatable nanoparticle with signal-amplification capabilities for non-invasive imaging of tumour malignancy. Nat Nanotechnol 11(8):724
Ni D, Shen Z, Zhang J, Zhang C, Wu R, Liu J et al (2016) Integrating anatomic and functional dual-mode magnetic resonance imaging: design and applicability of a bifunctional contrast agent. ACS Nano 10(3):3783–3790
Perrier M, Gallud A, Ayadi A, Kennouche S, Porredon C, Gary-Bobo M et al (2015) Investigation of cyano-bridged coordination nanoparticles Gd 3+/[Fe (CN) 6] 3−/d-mannitol as T 1-weighted MRI contrast agents. Nanoscale 7(28):11899–11903
Qin J, Liang G, Feng Y, Feng B, Wang G, Wu N et al (2020) Synthesis of gadolinium/iron–bimetal–phenolic coordination polymer nanoparticles for theranostic applications. Nanoscale 12(10):6096–6103
Shen Z, Chen T, Ma X, Ren W, Zhou Z, Zhu G et al (2017) Multifunctional theranostic nanoparticles based on exceedingly small magnetic iron oxide nanoparticles for T1-weighted magnetic resonance imaging and chemotherapy. ACS Nano 11(11):10992–11004
Shen Z, Song J, Zhou Z, Yung BC, Aronova MA, Li Y et al (2018) Dotted core–shell nanoparticles for T1-weighted MRI of tumors. Adv Mater 30(33):1803163
Shen Z, Fan W, Yang Z, Liu Y, Bregadze VI, Mandal SK et al (2019) Exceedingly small gadolinium oxide nanoparticles with remarkable relaxivities for magnetic resonance imaging of tumors. Small 15(41):1903422
Sherwood J, Rich M, Lovas K, Warram J, Bolding M, Bao Y (2017) T 1-Enhanced MRI-visible nanoclusters for imaging-guided drug delivery. Nanoscale 9(32):11785–11792
Struyfs H, Sima DM, Wittens M, Ribbens A, de Barros NP, Vân Phan T et al (2020) Automated MRI volumetry as a diagnostic tool for Alzheimer's disease: Validation of icobrain dm. NeuroImage Clin 26:102243
Sun Y, Kim HS, Kang S, Piao YJ, Jon S, Moon WK (2018) Magnetic resonance imaging-guided drug delivery to breast cancer stem-like cells. Adv Healthcare Mater 7(21):1800266
Tromsdorf UI, Bigall NC, Kaul MG, Bruns OT, Nikolic MS, Mollwitz B et al (2007) Size and surface effects on the MRI relaxivity of manganese ferrite nanoparticle contrast agents. Nano Lett 7(8):2422–2427

Wahsner J, Gale EM, Rodríguez-Rodríguez A, Caravan P (2018) Chemistry of MRI contrast agents: current challenges and new frontiers. Chem Rev 119(2):957–1057
Warsi MF, Adams RW, Duckett SB, Chechik V (2010) Gd-functionalised Au nanoparticles as targeted contrast agents in MRI: relaxivity enhancement by polyelectrolyte coating. Chem Commun 46(3):451–453
Yang H, Zhuang Y, Sun Y, Dai A, Shi X, Wu D et al (2011) Targeted dual-contrast T1-and T2-weighted magnetic resonance imaging of tumors using multifunctional gadolinium-labeled superparamagnetic iron oxide nanoparticles. Biomaterials 32(20):4584–4593
Zhang W, Liu L, Chen H, Hu K, Delahunty I, Gao S et al (2018) Surface impact on nanoparticle-based magnetic resonance imaging contrast agents. Theranostics 8(9):2521
Zhou Z, Lu ZR (2013) Gadolinium-based contrast agents for magnetic resonance cancer imaging. Wiley Interdiscip Rev Nanomed Nanobiotechnol 5(1):1–18
Zhou Z, Wu C, Liu H, Zhu X, Zhao Z, Wang L et al (2015) Surface and interfacial engineering of iron oxide nanoplates for highly efficient magnetic resonance angiography. ACS Nano 9(3):3012–3022
Zhou H, Guo M, Li J, Qin F, Wang Y, Liu T et al (2021) Hypoxia-triggered self-assembly of ultrasmall iron oxide nanoparticles to amplify the imaging signal of a tumor. J Am Chem Soc 143(4):1846–1853

Publisher's Note